Significantly improving the durability of single-chamber solid oxide fuel cells: a highly active CO_2-resistant perovskite cathode

Yuan Zhang,[†,‡] Xuechao Gao,[†] Jaka Sunarso,[§] Bo Liu,[†,‡] Wei Zhou,[,†,‡] Meng Ni[∥], Zongping Shao[*,†,‡,⊥]*

[†] Jiangsu National Synergetic Innovation Center for Advanced Materials (SICAM), State Key Laboratory of Materials-Oriented Chemical Engineering, Nanjing Tech University, Nanjing 210009, P. R. China

[‡] College of Chemical Engineering,, Nanjing Tech University, Nanjing 210009, P. R. China

[§] Research Centre for Sustainable Technologies, Faculty of Engineering, Computing and Science, Swinburne University of Technology, Jalan Simpang Tiga, Kuching 93350, Sarawak, Malaysia

[∥] Department of Building and Real Estate, The Hong Kong Polytechnic University, Hung Hom, Kowloon, Hong Kong 999077, China

[⊥] Department of Chemical Engineering, Curtin University, Perth, Western Australia 6845, Australia

KEYWORDS: Cathode; Oxygen reduction reaction; Perovskite; Single chamber SOFC; Solid oxide fuel cells

ABSTRACT: Single-chamber solid oxide fuel cell (SC-SOFC) represents an attractive alternative to battery for micropower application given its simplified stack design, easy gas management, lower operation temperature, and quicker start-up. Its stable operation over long duration relies on the availability of CO_2-resistant cathode materials with high oxygen reduction reaction activity. Here, we reported a novel perovskite oxide cathode $SrSc_{0.075}Ta_{0.025}Fe_{0.9}O_{3-\delta}$ (SSTF75), which provides CO_2 resistance and high ORR activity. A peak power density of 1430 mW cm^{-2} was achieved with SSTF75/$Sm_{0.2}Ce_{0.8}O_{1.9}$ cathode at 650 °C with a methane and oxygen gas mixture (1:1 vol. ratio). It retained stable voltage performance at 600 °C for over 90-hour duration when discharged at a current density of 1,000 mA cm^{-2}. This work not only represents an advancing step in the SC-SOFC field but also authenticates an effective co-doping strategy for the design of CO_2-resistant cathode for low temperature application.

Solid oxide fuel cells (SOFCs) bring the simultaneous advantages of high power density, high chemical to electrical energy conversion efficiency, fuel flexibility, and very low environmental emission to portable and stationary power generation applications.[1-2] For portable and micropower market segment where rapid start-up and high energy density become more crucial than obtaining maximum conversion efficiency, single-chamber solid oxide fuel cells (SC-SOFCs) are preferred over the conventional dual-chamber solid oxide fuel cells (DC-SOFCs) given its more compact cell stack, simpler manifold configuration, and self-sustaining temperature (from fuel oxidation by oxygen in air).[3-5] Their operating principle is based on the different catalytic activities of anode and cathode:[5]

$$\text{Anode}: CH_4 + 1/2O_2 \rightarrow 2H_2 + CO \quad \text{(I)}$$

$$H_2 + O^{2-} \rightarrow H_2O + 2e^- \quad \text{(II)}$$

$$\text{Cathode}: O_2 + 4e^- \rightarrow 2O^{2-} \quad \text{(III)}$$

$$\text{Full oxidation of methane: } CH_4 + 2O_2 \rightarrow 2H_2O + CO_2 \quad \text{(IV)}$$

In hydrocarbon-fueled SC-SOFCs case nonetheless, up to 10 vol. % CO_2 (of the chamber total volume) can be produced during operation.[6] In such a case, cathode materials such as $Ba_{0.5}Sr_{0.5}Co_{0.8}Fe_{0.2}O_{3-\delta}$ (BSCF), which are highly reactive to CO_2, especially below 900 °C, has a limited operation lifetime.[7, 8]

This highlights the need to develop CO_2-resistant cathode materials to support the development of practical SC-SOFCs that can retain stable and high performance over long operation lifetime.

The high reactivity of BSCF with CO_2 originates from the presence of alkaline earth metal cations (i.e., barium (Ba) and strontium (Sr)). The reaction of BSCF with CO_2 always leads to cathode performance degradation. For example, the performance of BSCF-based symmetric SOFC cell was reduced by 37-fold following the introduction of 10 vol. % of CO_2 into the air stream at 600 °C for only 15 min.[9] Compared with Ba^{2+} cation case, the presence of larger Sr^{2+} cation in the perovskite lattice displayed better stability in CO_2 atmosphere.[9, 10] Likewise, iron is better than cobalt given its lower basicity (or equivalently, higher acidity) which translates to higher CO_2 resistance.[11] Decreasing the electron density of the perovskite oxide ions is an effective way to lower its basicity. This can be attained by using metal cations that strongly draw the electron cloud away from oxygen anion, i.e., high oxidation state metal cations such as Nb^{5+} and Ta^{5+}.[12] These two cations were recently reported to also contribute positively towards the phase stability of several mixed ionic-electronic conductors (MIECs) perovskite oxides compositions.[13-15] Yi et al. developed a new CO_2-resistant perovskite composition $SrNb_{0.2}Fe_{0.8}O_{3-\delta}$ (SNF) whereas Zhu et al. developed a novel Ta-based perovskite composition $SrTa_{0.1}Fe_{0.9}O_{3-\delta}$ (STF); both of which showed long-term steady oxygen ionic transport performance in pure CO_2 atmosphere at 900 °C.[13, 16]

Current research trend shifts towards developing cobalt-free perovskite oxide cathodes for SOFCs application considering the extensive cost, compatibility, and stability issues of cobalt-based perovskite cathodes.[17-20] Doped $SrFeO_{3-\delta}$ (SF) perovskite oxide compositions such as A-site doped compositions of $(La,Sr)FeO_{3-\delta}$ and $(Bi,Sr)FeO_{3-\delta}$ and B-site doped compositions of $Sr(Nb,Fe)O_{3-\delta}$ and $Sr(Ti,Fe)O_{3-\delta}$ have been synthesized and tested, however; all of which showed lower cathode performances relative to cobalt-based perovskite cathodes.[21-26] Higher performance improvement margin is nonetheless still affordable, we projected to be attained *via* the synergistic effects (i.e., simultaneous optimization of the structure, the electronic property, and the redox chemistry) enabled by introducing particular co-dopants into the perovskite lattice. In this context, for example, we have demonstrated that Nb and Sc co-doped composition, i.e., $SrSc_{0.175}Nb_{0.025}Co_{0.8}O_{3-\delta}$ (SSNC) displayed very high ORR activity.[27] More recently, we highlighted the synergistic effects of Nb and Ta co-dopants on low temperature (below 500 °C) solid oxide fuel cell perovskite cathode with composition of $SrCo_{0.8}Nb_{0.1}Ta_{0.1}O_{3-\delta}$ (SCNT), which enables its stable and very high electrochemical performance below 500 °C.[28]

Here we report the synthesis and characterization of new high performance cobalt-free co-doped perovskite oxide cathode series, i.e., $SrSc_xTa_{0.1-x}Fe_{0.9}O_{3-\delta}$ (SSTF, x = 0, 0.025, 0.05, 0.075, and 0.1) for

intermediate temperature (500−650 °C) operation in SC-SOFC. Among these compositions, $SrSc_{0.075}Ta_{0.025}Fe_{0.9}O_{3-\delta}$ (SSTF75) cathode with $Sm_{0.2}Ce_{0.8}O_{1.9}$ (SDC) electrolyte for symmetric cell showed the lowest area specific resistance (ASR) of 0.092 Ω cm^2 at 600 °C in air. More importantly, by exploiting the combination of high ORR activity and CO_2 resistance of SSTF75/SDC composite cathode, a SC-SOFC achieved a high peak power density (PPD) of 1430 mW cm^{-2} at 650 °C. We also demonstrated stable voltage at 600 °C for over 90 hours. Our collective characterization results reveal that the presence of 7.5 mol. % of Sc^{3+} led to the high oxidation state for Fe and the formation of oxygen vacancies that promotes the ORR activity in SSTF75 while the presence of 2.5 mol. % of Ta^{5+} contributes to the enhanced CO_2 resistance for SSTF75. This work not only represents an advance in the SC-SOFC field but also underscores the efficacy of co-doping approach to overcome the current ORR performance limitations.

The room temperature powder X-ray diffraction (XRD) pattern of SSTF75 is compared against the powder XRD patterns of $SrSc_{0.1}Fe_{0.9}O_{3-\delta}$ (SSF) and STF in **Figure 1(a).** The complete powder XRD patterns for this series are displayed in **Figure S1**. Except for SSF, other samples show a weak peak just before the main peak (~32°), which indicates the ordered brownmillerite phase as observed in our previous work.[27] Other peaks can be indexed according to primitive perovskite phase with Pm-3m space group (#221). The positions of the characteristic peaks gradually shift to higher angle with the progressive increase in Ta^{5+} amount, i.e., in the order of SSF, SSTF75, $SrSc_{0.05}Ta_{0.05}Fe_{0.9}O_{3-\delta}$ (SSTF50), $SrSc_{0.025}Ta_{0.075}Fe_{0.9}O_{3-\delta}$ (SSTF25), and STF, indicating the reduction in the lattice parameter due to the smaller ionic radius of Ta^{5+} (0.64 Å) relative to that of Sc^{3+} (0.745 Å) (both at coordination number of 6).[29] Such observation denotes the successful doping of Sc^{3+} and Ta^{5+} into the perovskite lattice. Scanning electron microscopy-energy dispersive X-ray (SEM-EDX) elemental d istribution maps for Sr, Sc, Ta, Fe, and O on the surface of SSTF75 is displayed in **Figure 1(b)**. The primitive cubic structure of SSTF75 was further confirmed by high resolution transmission electron microscopy (HR-TEM) images along the two different zone axes, i.e., [111] and [100] (**Figure 1(c) and 1(d)**) and their corresponding selected area electron diffraction (SAED) patterns (Insets of **Figure 1(c) and 1(d)**).

The cathode thermal expansion coefficient (TEC) should match that of the electrolyte to reduce the tendency for the delamination of the cathode from the electrolyte during heating and cooling. The thermal expansion curves and the TECs of SSTF samples are shown in **Figure S2** and **Table S1**, respectively. Their TECs are lower than those of cobalt-containing perovskite oxides.[30-32] The phase stability of SSTF75 in a 10 vol. % CO_2-containing air atmosphere and ordinary air atmosphere were evaluated by performing *in situ* powder XRD analyses during heating and cooling between 25 and 900 °C as displayed

in **Figure 2(a)** and **Figure S3**, respectively. In CO_2-containing air atmosphere, a new impurity phase formed upon heating to 500 °C and disappeared when samples cooled down, indicating its reversible nature. The structure of SSTF75 was stable in both atmospheres. The phase reaction between SSTF75 cathode and SDC was also evaluated from the powder XRD pattern of their annealed powder mixture (**Figure 2(b)**). All peaks in the powder mixture can be attributed to the peaks from the two individual samples, thus ruling out the new phase formation from reaction between SSTF75 and SDC.

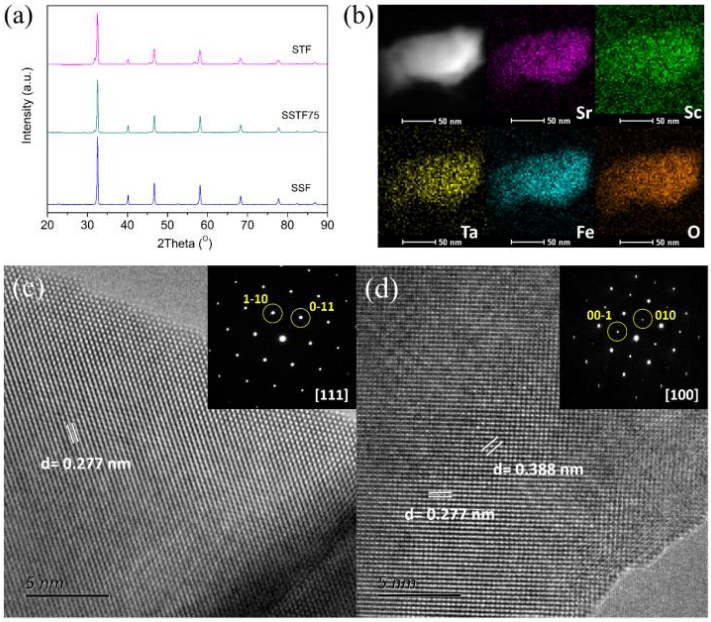

Figure 1. (a) Room temperature powder XRD patterns of SrTa0.1Fe0.9O3−δ□ (STF), SrSc0.075Ta0.025Fe0.9O3−δ (SSTF75), and SrSc0.1Fe0.9O3−δ□ (SSF) powders; **(b)** SEM-EDX elemental maps on the representative SSTF75 surface; and High-resolution TEM images along **(c)** [111] and **(d)** [100] zone axes of SSTF75 sample (Inset – the corresponding SAED patterns).

The electrical conductivity of SSTF75 between 300 and 900 °C displays a maximum value of 56 S cm^{-1} at 500 °C (**Figure S4**), which is significantly higher than that of $SrSc_{0.175}Nb_{0.025}Fe_{0.8}O_{3-\delta}$ (8.5 S cm^{-1} at 500 °C).[33] This suggests the more dominant contribution from Ta^{5+} towards the electrical conductivity enhancement relative to Nb^{5+}.

The ORR activities of SSTF on their symmetric cells configuration of SSTF|SDC|SSTF were evaluated by electrochemical impedance spectroscopy (EIS) shown in **Figure 3(a)**. The cathode layer thickness was maintained consistently at about 10 μm (**Figure S5**). Relative to the edge compositions, i.e., SSF and STF, the three Sc^{3+} and Ta^{5+} co-doped compositions showed lower area specific resistances (ASRs) at all tested temperatures. The best composition, i.e., SSTF75 exhibited the lowest ASR values of 0.25, 0.092, and 0.039 Ω cm^2 at 550, 600, and 650 °C, respectively. The superior performance of SSTF75 becomes more apparent at lower temperature. The typical impedance spectra for SSTF75 at five different temperatures, i.e., 550−750 °C are displayed in **Figure S6**. **Figure 3(b)** displays the temperature-

dependent Arrhenius plots of ASRs of SSTF75 in comparison to the other cobalt-free and cobalt-containing perovskite cathodes.[20,27,34-37] SSTF75 displayed ASRs values that fall within the lowest range observed for cobalt-free perovskite cathodes, which can only be surpassed by some cobalt-containing perovskite cathodes benchmarks.[27, 38]

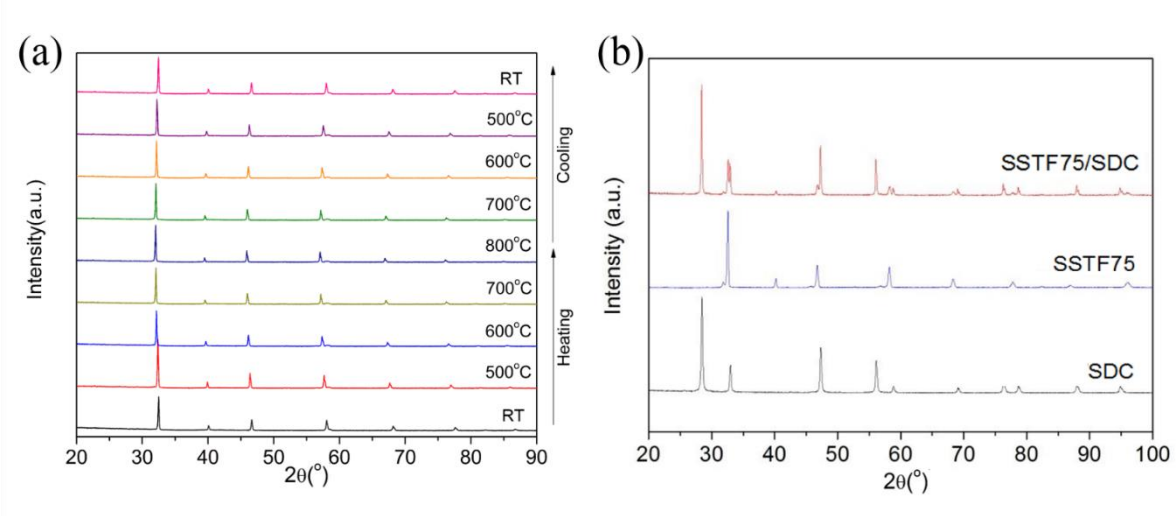

Figure 2. (a) High temperature powder XRD patterns of $SrSc_{0.075}Ta_{0.025}Fe_{0.9}O_{3-\delta}$ (SSTF75) during heating and cooling between 25 °C and 900 °C in 10 vol.% CO_2-containing air; and **(b)** Room temperature powder XRD patterns of $Sm_{0.2}Ce_{0.8}O_{1.9}$ (SDC), $SrSc_{0.075}Ta_{0.025}Fe_{0.9}O_{3-\delta}$ (SSTF75), and 1000 °C-calcined SSTF75 and SDC powder mixture (1:1 by weight) (SSTF75/SDC)..

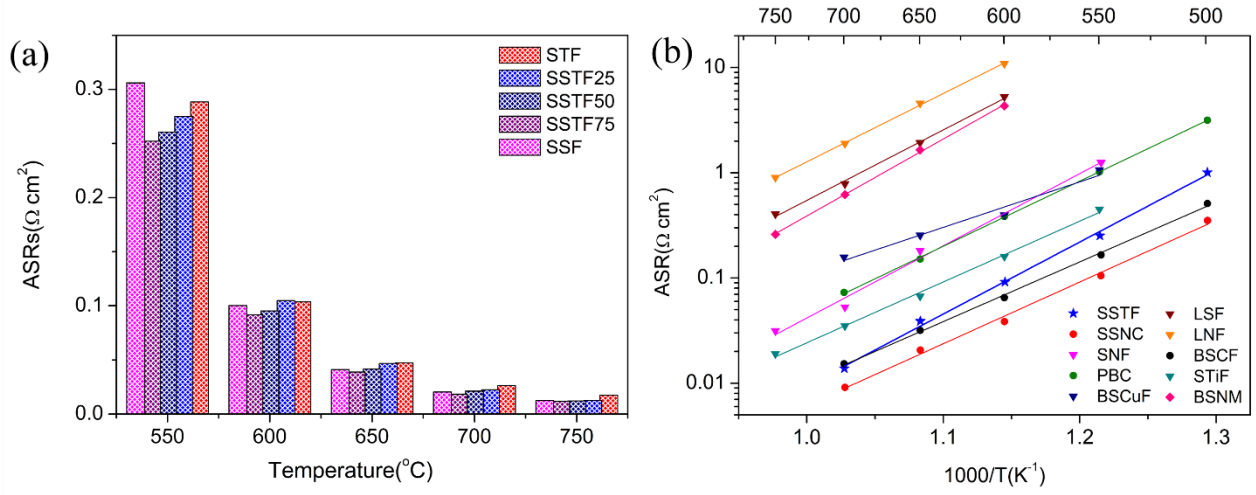

Figure 3. (a) The bar chart of the ASRs for $SrSc_{0.1}Fe_{0.9}O_{3-\delta}$□ (SSF), $SrSc_{0.075}Ta_{0.025}Fe_{0.9}O_{3-\delta}$ (SSTF75), $SrSc_{0.05}Ta_{0.05}Fe_{0.9}O_{3-\delta}$ (SSTF50), $SrSc_{0.025}Ta_{0.075}Fe_{0.9}O_{3-\delta}$ (SSTF25), and $SrTa_{0.1}Fe_{0.9}O_{3-\delta}$□ (STF) at 550 °C, 600 °C, 650 °C, 700 °C, and 750 °C; and **(b)** The temperature-dependent Arrhenius plots of ASRs of SSTF75 versus other cobalt-free and cobalt-containing perovskite cathodes. (SSTF: $SrSc_{0.075}Ta_{0.025}Fe_{0.9}O_{3-\delta}$; SSNC: $SrSc_{0.175}Nb_{0.025}Co_{0.8}O_{3-\delta}$; SNF: $SrNb_{0.1}Fe_{0.9}O_{3-\delta}$; PBC: $PrBaCo_2O_{5+\delta}$; BSCuF: $Ba_{0.5}Sr_{0.5}Fe_{0.8}Cu_{0.2}O_{3-\delta}$; LSF: $La_{0.5}Sr_{0.5}FeO_{3-\delta}$; LNF: $LaNi_{0.6}Fe_{0.4}O_{3-\delta}$; BSCF: $Ba_{0.5}Sr_{0.5}Co_{0.8}Fe_{0.2}O_{3-\delta}$; STiF: $SrTi_{0.1}Fe_{0.9}O_{3-\delta}$; BSNM: $Bi_2Sr_2Nb_2MnO_{12-\delta}$.)

As mentioned above, high ORR activity should also be accompanied by CO_2 resistance to substantiate cathode candidate's practical applicability in SC-SOFC.[9, 39] **Figure 4(a)** shows the comparative changes of ASRs after CO_2 was introduced to air stream and after the subsequent CO_2 removal. At 600 °C,

following 10 vol. % of CO_2 introduction for 15 minutes, the ASR of BSCF increased by 34-fold relative to its original ASR. For comparison, the ASR of SSTF75 developed in the present study only increased by 7-fold, indicating its significantly improved CO_2 resistance. SDC that exhibits low yet stable oxygen ionic transport performance in CO_2 atmosphere can be utilized as an additional cathode component.[28,40] The comparative change in ASRs of SSTF75/SDC composite cathode, i.e., SSTF75:SDC = 60:40 by weight is also depicted in **Figure 4(a)**. At 600 °C, this composite cathode shows slightly better CO_2 resistance than the individual SSTF75 cathode. **Figure 4(b)** presents more detailed observation into the ASR behavior of SSTF75/SDC composite cathode following exposure to 1, 5, and 10 vol. % of CO_2 and upon the subsequent CO_2 removal. In the perspective of obtaining simultaneous CO_2 resistance with SDC electrolyte, SSTF75/SDC composite cathode becomes the best cathode candidate for SC-SOFC test.

We additionally performed complementary characterizations to cross-check CO_2 resistance of SSTF75 against other compositions and BSCF. Powder XRD patterns, Fourier Transform Infra-Red (FTIR) spectra, and CO_2 temperature programmed desorption (CO_2-TPD) for SSTF after exposure to pure CO_2 atmosphere at 700 ºC for 2 hours were obtained (**Figure S7**) (details of which are given in the Supporting Information pS9-10). The average metal-oxygen bond energy (ABE) of a particular metal oxide estimated from thermodynamic calculations provides a quantitative indicator of its CO_2 resistance.[9] The ABEs values of SSF, SSTF75, SSTF50, SSTF25, and STF are −292, −295, −298, −301, and −304 kJ mol^{-1}, respectively (**Figure S8**). STF has the highest CO_2 resistance, which is consistent with its highest Ta content. These SSTF materials are chemically and structurally stable in CO_2-containing environment.

To gain an insight into the high ORR activity of SSTF75, we probed the oxygen non-stoichiometry (δ) and the average oxidation state of Fe in STF, SSTF75, and SSF *via* Mössbauer spectroscopy (**Figure S9**). The highest oxidation state for SSTF75 reflects the lowest electronegativity in Sc and Ta co-doped composition. Accordingly, the respective δ values for STF, SSTF75, and SSF are 0.216, 0.279, and 0.307. Higher Sc^{3+} content appears to increase the oxygen non-stoichiometry which benefits the ORR processes on the cathode of SOFCs. To gain more insights on this aspect, first principles simulations were performed to determine the crystal cell energies and oxygen vacancy formation energies of Sc-doped, Ta-doped, and Sc/Ta co-doped $SrFeO_3$ as displayed in **Figure 5**.[41-43] The molecular simulation calculation of the perovskite crystal cells was performed using the Vienna ab initio simulation package (VASP). For a given dopant at different dopant positions in **Figure 5(a)**, it had found that the doped supercell requires slightly higher energy than the Ta pure phase, the dopant ion is anticipated to adopt medium distance (MD) scenario. The dopant ion placement in MD scenario was then applied to evaluate the oxygen vacancy formation energy at different positions with respect to the dopant ions (**Figure S10**); the results of which

are shown in **Figure 5(b)**. The incorporation of Sc dopant into $SrFeO_3$ lattice led to lower oxygen vacancy formation energy than the incorporation of Ta dopant (**Figure 5(b)**) (Simulations details of which are given in the Supporting Information pS12-14). Based on the aforementioned analyses, we can conclude the synergetic effect of Sc and Ta in the Sc- and Ta- co-doped $SrFeO_{3-\delta}$ perovskites. The Sc doping increases the oxygen vacancy concentration which is responsible for the improvement of the ORR activity of the cathode. The Ta doping, on the other hand, increases the perovskites' acidity and ABE, which are two important aspects contributing to CO_2 resistance of the perovskite oxide.

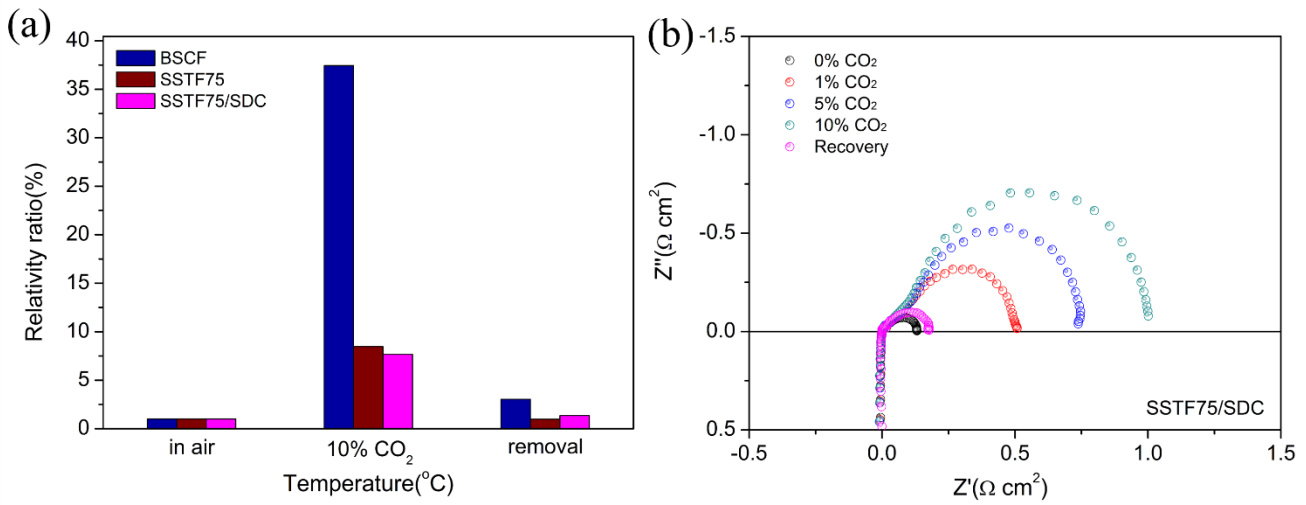

Figure 4. (a) The comparative changes of ASRs of BSCF, SSTF75, and SSTF75/SDC composite cathode (SSTF75:SDC = 60:40 by weight) at 600 °C after 10 vol. % CO_2 introduction to air stream and after the subsequent CO_2 removal for 30 minutes; and **(b)** Impedance spectra evolution of SSTF75/SDC composite cathode at 600 °C after exposure to air, 1 vol. %, 5 vol. %, and 10 vol. % of CO_2 and upon the subsequent CO_2 removal for 30 minutes.

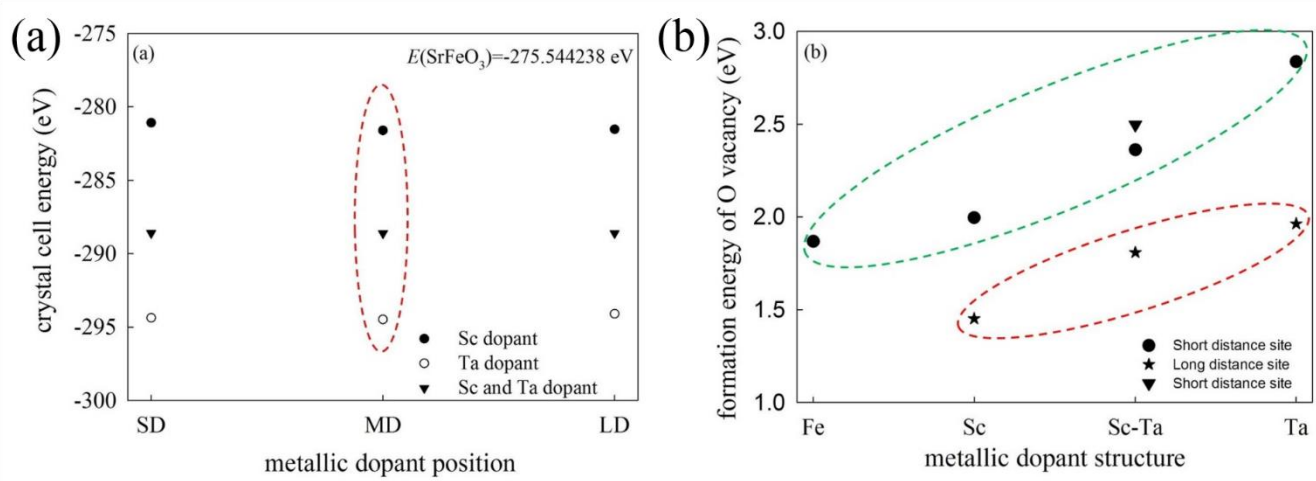

Figure 5. (a) Crystal cell energies of $SrFeO_3$ doped with Sc dopant, Ta dopant, and Sc and Ta co-dopants at different dopant positions(SD: short distance, MD: medium distance, LD: long distance); and **(b)** Oxygen vacancy formation energy at different dopant positions for different dopant cases (Fe, Sc, Sc-Ta, and Ta).

The electrochemical performance of SSTF75/SDC composite cathode in SC-SOFC was probed using a fuel cell with a configuration of (hydrogen reduced) Ni-YSZ (yttrium stabilized zirconia) tape casted anode | YSZ (12 μm) | SDC (5 μm) | SSTF75/SDC (10 μm) and a circular area of 0.48 cm^2; the cross-section of which is displayed in **Figure 6(a)**. The current-potential (I-V) polarization curve and the power density (I-P) curve for the cell were obtained under a methane/oxygen/nitrogen gas atmosphere (methane/oxygen total flow rate: 150 mL min^{-1}, nitrogen flow rate: 150 mL min^{-1}) between 500 and 650 °C. The occurrence of such reactions in the presence of CH_4 generally contributes to ~100 °C extra temperature rise from the furnace temperature.[35] The exact temperature rise, which determines the cell performance, depends on the ratio of CH_4 to O_2. Accordingly, we probed the power density at 600 °C as a function of O_2 to CH_4 volume ratio, as shown in **Figure 6(b)**. It is found that lower CH_4 to O_2 ratio increased the PPD. In fact, the decrease in CH_4 to O_2 ratio from 2 (10:5) to 1 (10:10) leads to a steady but significant increase in the PPD from 550 to 1280 mW cm^{-2} (**Figure 6(b)**). **Figure 6(c)** displays SSTF75/SDC-based fuel cell performance at a constant O_2 to CH_4 ratio of 1 (10:10) as a function of furnace temperature. The PPD increased from 700 to 1430 mW cm^{-2} as the furnace temperature rose from 500 °C to 650 °C. Accompanying the furnace temperature rise was the minor reduction in the open circuit voltage (OCV) from 0.93 V at 500 °C to 0.90 V at 700 °C. This OCV lowering came from the increasing temperature as well as possible the reduced selectivity of the cathode for ORR due to the enhanced catalytic activity for methane oxidation on the cathode surface at higher temperatures.[44] BSCF-based fuel cell exhibited substantially higher power density behavior but decreased more rapidly with increasing O_2:CH_4 ratio, relative to SSTF75-based fuel cell (Compare **Figure 6(b) and (c)** to **Figure S11(a) and (b)**). SSTF75-based fuel cell additionally showed stable voltage performance at 600 °C when discharged at a current density of 1000 mA cm^{-2} over the duration of 5,500 minutes (**Figure 6(d)**). For comparison, the voltage of a BSCF-based fuel cell continuously degraded substantially with increasing operation time. We attribute such performance deterioration to the reaction between BSCF and CO_2 that was generated during SC-SOFC operation.

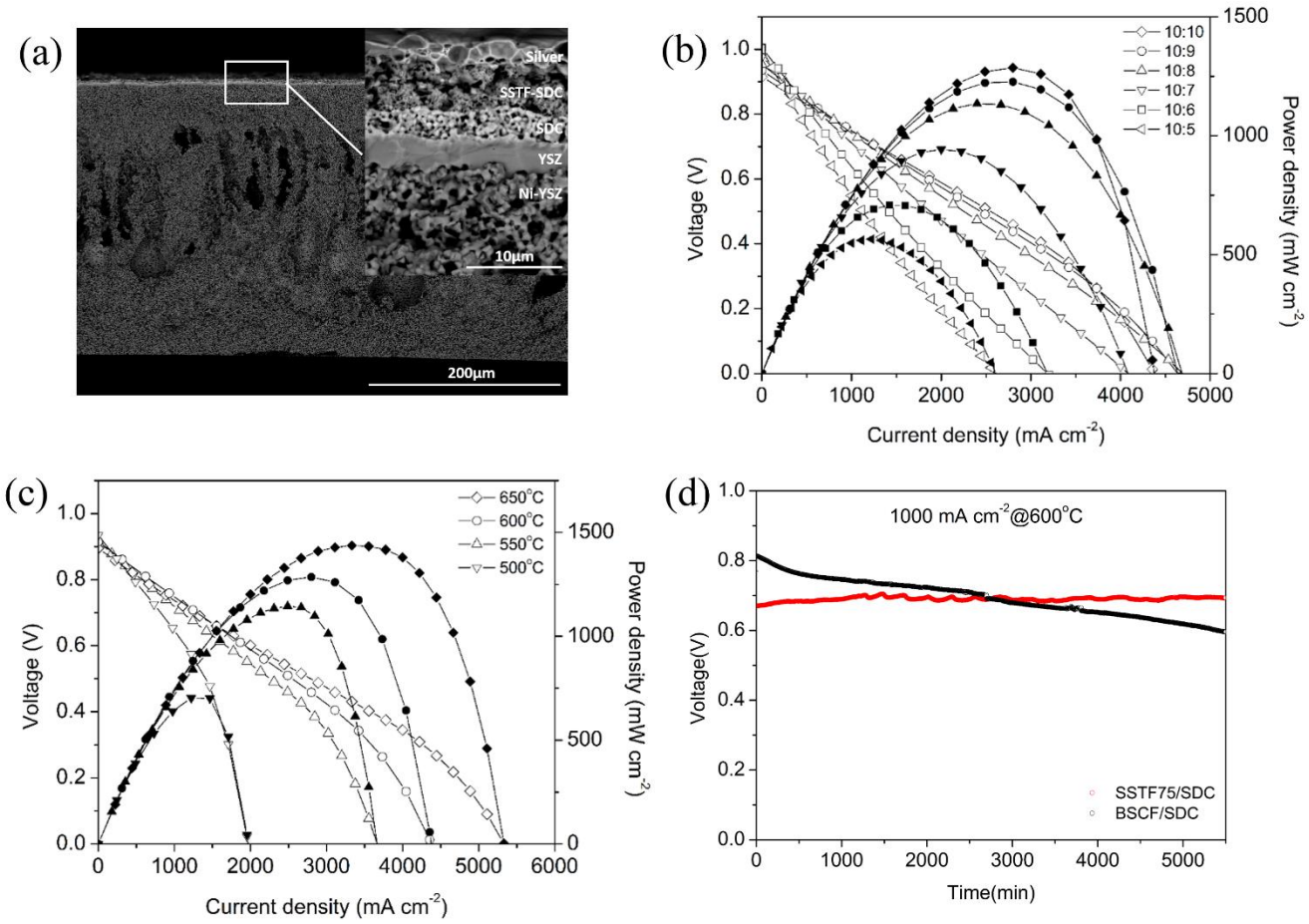

Figure 6. (a) SEM image of the cross-section of SSTF75/SDC composite cathode in SC-SOFC (Inset - The magnified view on the white rectangular section); **(b)** The current-potential (I-V) polarization and power density (I-P) curves of SSTF75/SDC-based fuel cell at 600 °C as a function of CH_4 to O_2 ratio from 10:5 to 10:10; **(c)** The current-potential (I-V) polarization and power density (I-P) curves of SSTF75/SDC-based fuel cell at an O_2 to CH_4 ratio of 1 (10:10) as a function of temperature from 500 to 650 °C; and **(d)** Time-dependent voltage profiles for SSTF75/SDC and BSCF/SDC-based fuel cells at 600 °C when discharged at a current rate of 1,000 mA cm^{-2} for 5500 minutes.

In summary, among these $SrSc_xTa_{0.1-x}Fe_{0.9}O_{3-\delta}$ (SSTF, x = 0, 0.025, 0.05, 0.075, and 0.1) compositions, $SrSc_{0.075}Ta_{0.025}Fe_{0.9}O_{3-\delta}$ (SSTF75) displayed the highest ORR activity as reflected by an ASR of 0.092 Ω cm^2 at 600 °C. SSTF75 also showed mild increase of ASR when 10 vol. % CO_2 was introduced into the air stream at 600 ºC for 15 min. SC-SOFC test was performed using SSTF75/SDC composite cathode-based fuel cell that exhibited a PPD of 1430 mW cm^{-2} at 650 °C under methane and oxygen (1:1 by volume) gas mixture atmosphere. This cell also maintained stable voltage performance over 90 h-period discharge test at 1000 mA cm^{-2} current density. First principles simulation showed that the high ORR activity contribution in SSTF75 comes from the presence of Sc^{3+} while the good CO_2 resistance comes from the presence of Ta^{5+}. Considering the limited fuel efficiency of SC-SOFC, the advance in cathode material progress we demonstrated here can be combined with the development of an efficient downstream catalyst in the same gas chamber to catalytically convert the unused methane gas into

synthesis gas, thus enabling the co-generation of electrical power and synthesis gas. In such a way, the potential of SC-SOFC for micropower application can be optimized and fitted into a specialized market segment not accessible to battery device.

ASSOCIATED CONTENT

Supporting Information

The Supporting Information is available free of charge on the ACS Publications website at DOI: xxxxxxxxx. Experimental Section and Supporting Figures and Tables including XRD, TEC, simulation calculation and electrochemical test and so on. (PDF)

AUTHOR INFORMATION

Corresponding Author

*E-mail: zhouwei1982@njtech.edu.cn (W. ZHOU). Tel.: +86 25 83172256; Fax: +86 25 83172242.

*E-mail: shaozp@njtech.edu.cn (Z.P. SHAO). Tel.: +86 25 83172256; Fax: +86 25 83172242.

Notes

The authors declare no competing financial interest.

ACKNOWLEDGMENTS

This work was financially supported by the National Nature Science Foundation of China (No. 21576135), Jiangsu Natural Science Foundation for Distinguished Young Scholars (No. BK20170043), the Priority Academic Program Development of Jiangsu Higher Education Institutions, the Program for Changjiang Scholars, the Program for Jiangsu Specially-Appointed Professors, and the Youth Fund in Jiangsu Province (No. BK20150945).

REFERENCES

[1] Steele, B. C. H.; Heinzel, A. Materials for Fuel-Cell Technologies. *Nature* **2001**, *414*, 345-352.

[2] Wachsman, E. D.; Marlowe, C. A.; Lee, K. T. Role of Solid Oxide Fuel Cells in a Balanced Energy Strategy. *Energy Environ. Sci.* **2012**, *5*, 5498-5509.

[3] Shao, Z. P.; Zhang, C. M.; Wang, W.; Su, C.; Zhou, W.; Zhu, Z. H.; Park, H. J.; Kwak, C. Electric Power and Synthesis Gas Co-generation From Methane with Zero Waste Gas Emission. *Angew. Chem. Int. Ed.* **2011**, *123*, 1832-1837.

[4] Hibino, T.; Hashimoto, A.; Inoue, T.; Tokuno, J. I.; Yoshida, S. I.; Sano, M. A Low-Operating-Temperature Solid Oxide Fuel Cell in Hydrocarbon-Air Mixtures. *Science* **2000**, *288*, 2031-2033.

[5] Rembelski, D.; Viricelle, J. P.; Combemale, L.; Rieu, M. Characterization and Comparison of Different Cathode Materials for SC-SOFC: LSM, BSCF, SSC, and LSCF. *Fuel Cells* **2012**, *12*, 256-264.

[6] Hao, Y.; Shao, Z. P.; Mederos, J.; Lai, W.; Goodwin, D. G.; Haile, S. M. Recent Advances in Single-Chamber Fuel-Cells: Experiment and Modeling. *Solid State Ionics* **2006**, *177*, 2013-2021.

[7] Yan, A. Y.; Cheng, M. J.; Dong, Y. L.; Yang, W. S.; Maragou, V.; Song, S. Q.; Tsiakaras, P. Investigation of a $Ba_{0.5}Sr_{0.5}Co_{0.8}Fe_{0.2}O_{3-\delta}$ Based Cathode IT-SOFC: I. The Effect of CO_2 on the Cell Performance. *Appl. Catal. B* **2006**, *66*, 64-71.

[8] Liu, B.; Chen, X.; Dong, Y.; Mao, S. S.; Cheng, M. A High-Performance, Nanostructured $Ba_{0.5}Sr_{0.5}Co_{0.8}Fe_{0.2}O_{3-\delta}$ Cathode for Solid-Oxide Fuel Cells. *Adv. Energy Mater.* **2011**, *1*, 343-346.

[9] Zhang, Y.; Yang, G.; Chen, G.; Ran, R.; Zhou, W.; Shao, Z. Evaluation of the CO_2 Poisoning Effect on a Highly Active Cathode $SrSc_{0.175}Nb_{0.025}Co_{0.8}O_{3-\delta}$ in the Oxygen Reduction Reaction. *ACS Appl. Mater. Interfaces* **2016**, *8*, 3003-3011.

[10] Yáng, Z.; Harvey, A. S.; Gauckler, L. J. Influence of CO_2 on $Ba_{0.2}Sr_{0.8}Co_{0.8}Fe_{0.2}O_{3-\delta}$ at Elevated Temperatures. *Scripta Materialia* **2009**, *61*, 1083-1086.

[11] Zhu, Y. L.; Sunarso, J.; Zhou, W.; Shao, Z. P. Probing CO_2 Reaction Mechanisms and Effects on the $SrNb_{0.1}Co_{0.9-x}Fe_xO_{3-\delta}$ Cathodes for Solid Oxide Fuel Cells. *Appl. Catal. B* **2015**, *172*, 52-57.

[12] Zhang, C.; Sunarso, J.; Liu, S. Designing CO_2-Resistant Oxygen-Selective Mixed Ionic-Electronic Conducting Membranes: Guidelines, Recent Advances, and Forward Directions. *Chem. Soc. Rev.* **2017**, *46*, 2941-3005.

[13] Yi, J.; Schroeder, M.; Weirich, T.; Mayer, J. Behavior of Ba (Co, Fe, Nb) $O_{3-\delta}$ Perovskite in CO_2-Containing Atmospheres: Degradation Mechanism and Materials Design. *Chem. Mater.* **2010**, *22*, 6246-6253.

[14] Nagai, T.; Ito, W.; Sakon, T. Relationship between Cation Substitution and Stability of Perovskite Structure in $SrCoO_{3-\delta}$-Based Mixed Conductors. *Solid State Ionics* **2007**, *177*, 3433-3444.

[15] Chen, W.; Chen, C.; Bouwmeester, H. J. M.; Nijmeijer, A.; Winnubst, L. Oxygen-Selective Membranes Integrated with Oxy-Fuel Combustion. *J. Membr. Sci.* **2014**, *463*, 166-172.

[16] Zhu, J.; Guo, S.; Chu, Z.; Jin, W. CO_2-Tolerant Oxygen-Permeable Perovskite-Type Membranes with High Permeability. *J. Mater. Chem. A* **2015**, *3*, 22564-22573.

[17] Hou, S.; Alonso, J. A.; Goodenough, J. B. Co-free, Iron Perovskites as Cathode Materials for Intermediate-Temperature Solid Oxide Fuel Cells. *J. Power Sources* **2010**, *195*, 280-284.

[18] Ma, Z. H.; Sun, C. W.; Ma, C.; Wu, H.; Zhan, Z. L.; Chen, L. Q. Ni Doped $La_{0.6}Sr_{0.4}FeO_{3-\delta}$ Symmetrical Electrode for Solid Oxide Fuel Cells. *Chinese J. Catal.* **2016**, *37*, 1347-1353.

[19] Sun, C. W.; Hui, R.; Roller, J. Cathode Materials for Solid Oxide Fuel Cells: A Review. *J. Solid State Electrc.* **2010**, *14*, 1125-1144.

[20] Jiang, S. S.; Sunarso, J.; Zhou, W.; Shen, J.; Ran, R.; Shao, Z. P. Cobalt-Free $SrNb_xFe_{1-x}O_{3-\delta}$ (x = 0.05, 0.1 and 0.2) Perovskite Cathodes for Intermediate Temperature Solid Oxide Fuel Cells. *J. Power Sources* **2015**, *298*, 209-216.

[21] Simner, S. P.; Bonnett, J. F.; Canfield, N. L.; Meinhardt, K. D.; Shelton, J. P.; Sprenkle, V. L. Development of Lanthanum Ferrite SOFC Cathodes. *J. Power Sources* **2003**, *113*, 1-10.

[22] Niu, Y.; Liang, F. L.; Zhou, W.; Sunarso, J.; Zhu, Z. H.; Shao, Z. P. A Three-Dimensional Highly Interconnected Composite Oxygen Reduction Reaction Electrocatalyst Prepared from a Coreeshell Precursor. *ChemSusChem* **2011**, *4*, 1582-1586.

[23] Wedig, A.; Merkle, R.; Stuhlhofer, B.; Habermeier, H.; Maier, J.; Heifets, E. Fast Oxygen Exchange Kinetics of Pore-Free $Bi_{1-x}Sr_xFeO_{3-\delta}$ Thin Films. *Phys. Chem. Chem. Phys.* **2011**, *13*, 16530-16533.

[24] Zhou, Q. J.; Zhang, L. L.; He, T. M. Cobalt-Free Cathode Material $SrFe_{0.9}Nb_{0.1}O_{3-\delta}$ for Intermediate-Temperature Solid Oxide Fuel Cells. *Electrochem. Commun.* **2010**, *12*, 285-287.

[25] Jiang, S. S.; Liang, F. L.; Zhou, W.; Shao, Z. P. Hierarchical Porous Cobalt-Free Perovskite Electrode for Highly Efficient Oxygen Reduction. *J. Mater. Chem.* **2012**, *22*, 16214-16218.

[26] Yu, X. L.; Long, W.; Jin, F. J.; He, T. M. Cobalt-Free Perovskite Cathode Materials $SrFe_{1-x}Ti_xO_{3-\delta}$ and Performance Optimization for Intermediate-Temperature Solid Oxide Fuel Cells. *Electrochem. Acta* **2014**, *123*, 426-434.

[27] Zhou, W.; Sunarso, J.; Zhao, M. W.; Liang, F. L.; Klande, T.; Feldhoff, A. A Highly Active Perovskite Electrode for the Oxygen Reduction Reaction Below 600°C. *Angew. Chem. Int. Ed.* **2013**, *52*, 14036-14040.

[28] Li, M.; Zhou, W.; Zhu, Z. Highly CO_2-Tolerant Cathode for Intermediate-Temperature Solid Oxide Fuel Cells: Samarium-Doped Ceria-Protected $SrCo_{0.85}Ta_{0.15}O_{3-\delta}$ Hybrid. *ACS Appl. Mater. Interfaces* **2017**, *9*, 2326-2333.

[29] Shannon, R. D. Revised Effective Ionic Radii and Systematic Studies of Interatomic Distances in Halides and Chalcogenides. *Acta Cryst.* **1976**, *A32*, 751-767.

[30] Wang, F.; Zhou, Q.; He, T.; Li, G.; Ding, H. Novel $SrCo_{1-y}Nb_yO_{3-\delta}$ Cathodes for Intermediate-Temperature Solid Oxide Fuel Cells. *J. Power Sources* **2010**, *195*, 3772-3778.

[31] Vente, J. F.; McIntosh, S.; Haije, W. G.; Bouwmeester, H. J. M. Properties and Performance of $Ba_xSr_{1-x}Co_{0.8}Fe_{0.2}O_{3-\delta}$ Materials for Oxygen Transport Membranes. *J. Solid State Electrochem.* **2006**, *10*, 581-588.

[32] Pikalova, E. Y.; Maragou, V. I.; Demina, A. N.; Demin, A. K.; Tsiakaras, P. E. The Effect of Co-Dopant Addition on the Properties of $Ln_{0.2}Ce_{0.8}O_{2-\delta}$ (Ln= Gd, Sm, La) Solid-State Electrolyte. *J. Power Sources* **2008**, *181*, 199-206.

[33] Chen, G.; Wang, Y.; Sunarso, J.; Liang, F.; Wang, H. A New Scandium and Niobium Co-doped Cobalt-Free Perovskite Cathode for Intermediate-Temperature Solid Oxide Fuel Cells. *Energy* **2016**, *95*, 137-143.

[34] Yang, G.; Su, C.; Chen, Y. B.; Dong, F. F.; Tade, M. O.; Shao, Z. P. Cobalt-Free $SrFe_{0.9}Ti_{0.1}O_{3-\delta}$ as a High-Performance Electrode Material for Oxygen Reduction Reaction on Doped Ceria Electrolyte with Favorable CO_2 Tolerance. *J. Eur. Ceram. Soc.* **2015**, *35*, 2531-2539.

[35] Kim, G.; Wang, S.; Jacobson, A. J.; Reimus, L.; Brodersen, P.; Mims, C. A. Rapid Oxygen Ion Diffusion and Surface Exchange Kinetics in $PrBaCo_2O_{5+x}$ with a Perovskite Related Structure and Ordered A Cations. *J. Mater. Chem.* **2007**, *17*, 2500-2505.

[36] Niu, Y. J.; Sunarso, J.; Liang, F. L.; Zhou, W.; Zhu, Z. H.; Shao, Z. P. A Comparative Study of Oxygen Reduction Reaction on Bi-and La-doped $SrFeO_{3-\delta}$ Perovskite Cathodes. *J. Electrochem. Soc.* **2011**, *158*, B132-B138.

[37] Zhu, Y.; Zhou, W.; Chen, Y.; Shao, Z. An Aurivillius Oxide Based Cathode with Excellent CO_2 Tolerance for Intermediate-Temperature Solid Oxide Fuel Cells. *Angew. Chem. Int. Ed.* **2016**, *55*, 8988-8993.

[38] Shao, Z. P.; Haile, S. M. A High-Performance Cathode for the Next Generation of Solid-Oxide Fuel Cells. *Nature* **2004**, *431*, 170-173.

[39] Bucher, E.; Egger, A.; Caraman, G. B.; Sitte, W. Stability of the SOFC Cathode Material (Ba, Sr)(Co, Fe) $O_{3-\delta}$ in CO_2-Containing Atmospheres. *J. Electrochem. Soc.* **2008**, *155*, B1218-B1224.

[40] Zhang, K.; Meng, B.; Tan, X.; Liu, L.; Wang, S.; Liu, S. CO_2-Tolerant Ceramic Membrane Driven by Electrical Current for Oxygen Production at Intermediate Temperatures. *J. Am. Ceram. Soc.* **2014**, *97*, 120-126.

[41] Dyer, M. S.; Collins, C.; Hodgeman, D.; Chater, P. A.; Demont, A.; Romani, S.; Sayers, R.; Thomas, M. F.; Claridge, J. B.; Darling, G. R.; Rosseinsky, M. J. Computationally Assisted Identification of Functional Inorganic Materials. *Science* **2013**, *340*, 847-852.

[42] Deml, A. M.; Stevanovic, V.; Muhich, C. L.; Musgrave, C. B.; O'Hayre, R. Oxide Enthalpy of Formation and Band Gap Energy as Accurate Descriptors of Oxygen Vacancy Formation Energetics. *Energy Environ. Sci.* **2014**, *7*, 1996-2004.

[43] Kuklja, M. M.; Kotomin, E. A.; Merkle, R.; Mastrikov, Y. A.; Maier, J. Combined Theoretical and Experimental Analysis of Processes Determining Cathode Performance in Solid Oxide Fuel Cells. *Phys.Chem. Chem. Phys.* **2013**, *15*, 5443-5471.

[44] Shao, Z.; Mederos, J.; Chueh, W. C.; Haile, S. M. High Power-Density Single-Chamber Fuel Cells Operated on Methane. *J. Power Sources* **2006**, *162*, 589-596.

SYNOPSIS TOC: **A novel and effective co-doping strategy perovskite cathode** towards the application of single-chamber solid oxide fuel cell was proposed for the first time to achieve high ORR catalytic activity and stable performance, meanwhile provide strong CO_2 resistance for intermediate temperature.